LOCALIZATION OF AERIAL VEHICLES PERFORMING AGGRESSIVE MANEUVERS IN GPS-UNRELIABLE ENVIRONMENTS USING VISION INFORMATION AND ADAPTIVE STATE ESTIMATORS

Antonio C. B. Chiella*, Bruno O. S. Teixeira*, Guilherme A. S. Pereira*

*Graduate Program in Electrical Engineering, Federal University of Minas Gerais
Av. Antônio Carlos 6627, 31270-901, Belo Horizonte, MG, Brazil

Emails: acbchiella@ufmg.br, brunoot@ufmg.br, gpereira@ufmg.br

Abstract— This paper considers the problems of localization and flight path reconstruction of aerial vehicles in GPS-unreliable environments. Our motivation comes from aerobatics competitions and aerial races, where the GPS signal can be lost during the execution of aggressive maneuvers, or damaged due to the strong interference caused by the digital television transmitters installed on the aircraft. Despite these problems, a good path estimate in such situations would be helpful for the pilot to improve the flight performance. In this paper, we investigate two adaptive filters and smothers based on the unscented Kalman filter/smoother. Aiming at a better path estimate, we also propose the inclusion of vision information obtained from the onboard camera. Experimental data collected from an airplane flying in a session of the Red Bull Air Race is used to illustrate the performance of the methods. Substantial improvements are observed when the adaptive algorithms and camera information are used for the vehicle localization and the reconstruction of its path.

Keywords— Adaptive Kalman filtering, Localization, Flight path reconstruction.

1 Introduction

Localization and flight path reconstruction of aerial vehicles are usually performed by combining Global Positioning System (GPS) data with Inertial Navigation System (INS) and compass (Leutenegger and Siegwart, 2012). INS and compass provides high frequency information, but INS accuracy deteriorates with the time due sensor biases and noise. On the other hand, GPS provides accurate absolute position and velocity at low frequency. Standard solutions that use recursive filters to predict the movement of the vehicle using INS, and GPS and compass to correct this prediction in a lower rate (Teixeira et al., 2011).

The standard solution usually works very well when the vehicle is flying at high altitudes in a leveled flight. However, when the flight happens close to the ground, in the presence of buildings and mountains, or when the vehicle performs acrobatic maneuvers, the GPS satellite signal may be blocked, causing the data to be unreliable or even unavailable. The motivation for this work came from aerial races and aerobatics competitions, when, besides all of these situations, the presence of strong television signals may also jam the GPS signal. Although localization is not very important in such competitions, a good flight path reconstruction may make a big difference for the pilots that want to improve their performance.

GPS-denied aerial flight has become a popular research topic, especially in the area of robotics (Bachrach et al., 2010; Chambers et al., 2011). In environments where GPS is unreliable or unavailable, it is necessary to estimate velocity and position using extereoceptive sensors, such as cameras and lasers, because available proprioceptive sensors, such as INS and compass, are not accurate enough (Shen et al., 2014).

Approximations based on the Kalman filter (KF), like the extended Kalman filter (EKF) and unscented Kalman filter (UKF), have been widely used in sensor fusion. However, it is difficult to assign suitable statistical properties to both the dynamic and observation models in some conditions, which include aerial-GPS navigation, where the maneuver of the vehicle and the level of measurement noise are environment-dependent and hardly predicted. When the GPS measurement noise changes, the filter performance degrades seriously. Therefore, to assign constant noise levels for such applications is not realistic (Hu et al., 2003).

To improve the performance of Kalman based algorithms, one possible approach is to modify online their stochastic parameters, which is known as adaptive Kalman filtering. To achieve that, different schemes are employed in the literature for the localization problem. Noise covariance scaling was investigated in (Hu et al., 2003; Hide et al., 2004). Based on multiple filters running in parallel, an approach called Multiple Model Adaptive Estimation (MMAE) was studied in (Hide et al., 2004; Abuhashim et al., 2010). For rapid maneuvers and multiple modes of operation, the Interacting Multiple Model (IMM) estimator was investigated in (Jwo and Tseng, 2011).

In this work, the localization problem of an aerial vehicle flying near the ground is investigated. To obtain state estimates on GPS-unreliable areas, two adaptive filtering approaches, namely noise covariance scaling and IMM are tested using actual data. In order to improve the estimation and obtain a smoother estimated path off-line, the adaptive approaches are also combined with a smoother algorithm to solve the vehicle's flight path reconstruction (FPR) problem (Teixeira et al., 2011).

2 Problem Statement

We address the problem of localization of an aerial vehicle flying near the ground. Thus, a set of aircraft sensor data is fused to generate a smooth state estimate of the path performed by the vehicle. This problem can be cast as a general nonlinear state estimation problem.

We assume that the available data is provided by the following instruments: 3-axis accelerometer measuring linear accelerations $A_{x,\mathrm{m}}$, $A_{y,\mathrm{m}}$ and $A_{z,\mathrm{m}}$; 3-axis gyroscope measuring the angular velocity components p_m, q_m and r_m; barometer measuring the absolute pressure and consequently the altitude H_m; Pitot tube measuring the airspeed $V_{TAS,\mathrm{m}}$; attitude and heading reference system (AHRS) providing the orientation angles ϕ_m, θ_m and ψ_m; GPS measuring the absolute position $x_{E,\mathrm{m}}$ and $y_{E,\mathrm{m}}$ and; camera providing images similar to the pilot view. From camera data, it is possible to obtain the moment at which the airplane pass by georeferenced landmarks, thereby obtaining absolute position $x_{E,\mathrm{g}}$ and $y_{E,\mathrm{g}}$.

The information provided by GPS and camera are sampled at a lower rate, yielding different combinations of measurements and, consequently, different observation models. The GPS measurements sometimes becomes unreliable due to the aggressive maneuvers of the airplane or interference caused by the digital television transmitters.

3 Mathematical Modeling

3.1 Nonlinear State Estimation

Consider the nonlinear stochastic discrete-time dynamic system

$$x_k = f\left(x_{k-1},\, u_{k-1},\, w_{k-1},\, k-1\right), \tag{1}$$

$$y_k = h\left(x_k,\, k\right) + v_k, \tag{2}$$

where $f : \mathbb{R}^n \times \mathbb{R}^p \times \mathbb{R}^q \times \mathbb{N} \to \mathbb{R}^n$ and $h : \mathbb{R}^n \times \mathbb{N} \to \mathbb{R}^m$ are the process and measurement models, respectively, $x_k \in \mathbb{R}^n$ is de state vector, $u_{k-1} \in \mathbb{R}^p$ is the input vector, $y_k \in \mathbb{R}^m$ is the measurement vector, $w_{k-1} \in \mathbb{R}^q$ and $v_k \in \mathbb{R}^r$ are, respectively, the process and measurement noise random vectors and k denotes discrete time. Assume that, for all $k \geq 1$, the know data are the measurements y_k, the input u_{k-1}, $\hat{x}_{0|0} = E[x_0]$, and $P^{xx}_{0|0} = E[(x_0 - \hat{x}_{0|0})(x_0 - \hat{x}_{0|0})^T]$, where $x_0 \in \mathbb{R}^n$ is the initial state vector and $E[\cdot]$ denotes the expected value. Furthermore, consider that w_{k-1} and v_k have zero mean, known covariance matrices Q_{k-1} and R_k, respectively, and are assumed to be mutually independent. Under the stated assumptions, given the models (1) and (2) and the sequence of past and present measured data $y_1, ..., y_k$, the state-estimation problem is to find the estimate $\hat{x}_{k|k} = E[x_k]$ and covariance $P^{xx}_{k|k} = E[(x_k - \hat{x}_{k|k})(x_k - \hat{x}_{k|k})^T]$ that characterizes the *posterior* PDF $\rho(x_k|(y_1...y_k))$. In general, for nonlinear systems, the solution to this problem can be quite complex, due the fact that *posterior* probability density function (PDF) could not be completely characterized by its mean $\hat{x}_{k|k}$ and covariance matrix $P^{xx}_{k|k}$. Thus, approximations based on the unscented Kalman filter (UKF) are used (Julier and Uhlmann, 2004).

3.2 Kinematic Modeling

Based on the kinematic model of airplanes (Beard and McLain, 2012), and the available sensors, we define the state vector $x(t) \in \mathbb{R}^{16}$ as a concatenation of the vectors

$$x_s \triangleq [u \;\; v \;\; w \;\; e_0 \;\; e_1 \;\; e_2 \;\; e_3 \;\; x_E \;\; y_E \;\; z_E]^T, \tag{3}$$

$$x_b \triangleq \left[b_{A_x} \;\; b_{A_y} \;\; b_{A_z} \;\; b_p \;\; b_q \;\; b_r\right]^T, \tag{4}$$

where $x_s(t) \in \mathbb{R}^{10}$ form the nonlinear process model of an airplane in state space and $x_b(t) \in \mathbb{R}^6$ are the bias variables of the accelerometers and gyrometers, thereby compounding a joint estimation of states and parameters.

The accelerations measured by the accelerometers and the angular rates measured by the gyrometers play the role of inputs $u_{k-1} \in \mathbb{R}^6$

$$u \triangleq [A_{x,\mathrm{m}} \;\; A_{y,\mathrm{m}} \;\; A_{z,\mathrm{m}} \;\; p_\mathrm{m} \;\; q_\mathrm{m} \;\; r_\mathrm{m}]^T, \tag{5}$$

where the subscript "m" denotes onboard measurements.

The state-space dynamical model is completed by considering the observation equations whose measurement vector $y_k \in \mathbb{R}^{10}$ can be formed by

$$y_k \triangleq [e_\mathrm{m} \;\; V_{TAS,\mathrm{m}} \;\; x_{E,\mathrm{m}} \;\; y_{E,\mathrm{m}} \;\; H_\mathrm{m} \;\; x_{E,\mathrm{g}} \;\; y_{E,\mathrm{g}}]^T, \tag{6}$$

where the subscript "g" denotes the camera information, and the components of unit quaternion $e_\mathrm{m} = [e_{0,\mathrm{m}}\, e_{1,\mathrm{m}}\, e_{2,\mathrm{m}}\, e_{3,\mathrm{m}}]^T \in \mathbb{R}^4$ are obtained from the unscented transform of Euler angles, which are provided by the AHRS as in (Terra et al., 2014). Note that, the measurement vector can change depending on the available sensors.

The state-space equation used in the localization problem is given by (omitting the argument t on right-hand side)

$$\dot{x}_s(t) = \begin{bmatrix} rv - qw - 2g(e_1e_3 - e_0e_2) + A_x \\ -ru + pw + 2g(e_2e_3 + e_0e_1) + A_y \\ qu - pv + g(e_0^2 - e_1^2 - e_2^2 + e_3^2) + A_z \\ -\frac{1}{2}(pe_1 + qe_2 + re_3) \\ -\frac{1}{2}(-pe_0 - re_2 + qe_3) \\ -\frac{1}{2}(-qe_0 + re_1 - pe_3) \\ -\frac{1}{2}(-re_0 - qe_1 + pe_2) \\ \mathrm{row}_1\left(\mathcal{R}_B^{NED}\right)[u\; v\; w]^T \\ \mathrm{row}_2\left(\mathcal{R}_B^{NED}\right)[u\; v\; w]^T \\ \mathrm{row}_3\left(\mathcal{R}_B^{NED}\right)[u\; v\; w]^T \end{bmatrix} + \begin{bmatrix} w_u \\ w_v \\ w_w \\ w_{e_0} \\ w_{e_1} \\ w_{e_2} \\ w_{e_3} \\ w_{x_E} \\ w_{y_E} \\ w_{z_E} \end{bmatrix} \tag{7}$$

and the bias terms are modeled as a random-walk process,

$$\dot{x}_b(t) = w_b \in \mathbb{R}^6, \tag{8}$$

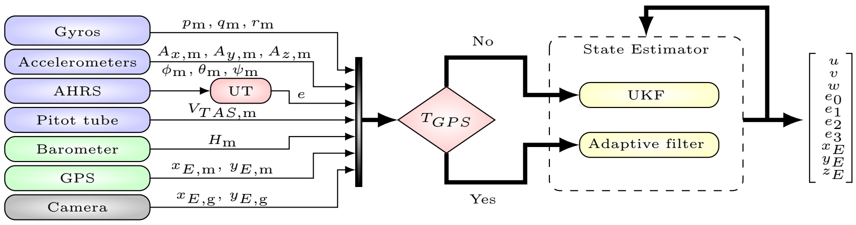

Figure 1: Block diagram of the localization procedure. In purple color, the high frequency (50Hz) sampled data, the low frequency (5Hz) sampled data in green, the processed data from camera in gray, the preprocessing data in red and the filtering algorithms in yellow. The choice between the adaptive algorithm and the standard UKF is done by the GPS time sample T_{GPS}.

where $\mathcal{R}_B^{NED}$ is the orthogonal matrix that relates the rigid body and the north-east-down (NED) reference frame.

Define the noise vector due to the input u_{k-1} as $w_1 = [w_{A_x}\, w_{A_y}\, w_{A_z}\, w_p\, w_q\, w_r]^T \in \mathbb{R}^6$, with covariance matrix $Q_{1,k-1} \in \mathbb{R}^{6\times 6}$, and the additive process noise vector as $w_2 = [w_s^T \quad w_b^T]^T \in \mathbb{R}^{16}$, with covariance matrix $Q_{2,k-1} = \begin{bmatrix} Q_s & 0_{10\times 6} \\ 0_{6\times 10} & Q_b \end{bmatrix} \in \mathbb{R}^{16\times 16}$, where $w_s = [w_u\, w_v\, w_w\, w_{e_0}\, w_{e_1}\, w_{e_2}\, w_{e_3}\, w_{x_E}\, w_{y_E}\, w_{z_E}]^T \in \mathbb{R}^{10}$ models unknown disturbances and improves the stability of the algorithm, and $w_b = [w_{b_{A_x}}\, w_{b_{A_y}}\, w_{b_{A_z}}\, w_{b_p}\, w_{b_q}\, w_{b_r}]^T \in \mathbb{R}^6$ models the Gaussian random walk of the accelerometer and gyroscope bias. Note that, the inputs (5) discount the respective bias and noise (for example, $r = r_m - r_b - w_r$) in (7).

In order to obtain (1), the state-space equations are discretized by integrating (7)-(8) over the time interval $[(k-1)T; kT]$, however, only the right-hand end-point of $[(k-1)T; kT]$ given by $x_k \triangleq x(kT)$ is used.

The measurement model (2) is given by

$$y_k = \begin{bmatrix} e_0 \\ e_1 \\ e_2 \\ e_3 \\ \sqrt{u^2+v^2+w^2} \\ x_E \\ y_E \\ -z_E \\ x_E \\ y_E \end{bmatrix} + \begin{bmatrix} r_{e_{0,\mathrm{m}}} \\ r_{e_{1,\mathrm{m}}} \\ r_{e_{2,\mathrm{m}}} \\ r_{e_{3,\mathrm{m}}} \\ r_{V_{TAS,\mathrm{m}}} \\ r_{x_{E,\mathrm{m}}} \\ r_{y_{E,\mathrm{m}}} \\ r_{H_{\mathrm{m}}} \\ r_{x_{E,\mathrm{g}}} \\ r_{y_{E,\mathrm{g}}} \end{bmatrix}, \quad (9)$$

where $v_k = [r_{e_{0,\mathrm{m}}}\, r_{e_{1,\mathrm{m}}}\, r_{e_{2,\mathrm{m}}}\, r_{e_{3,\mathrm{m}}}\, r_{V_{TAS,\mathrm{m}}}\, r_{x_{E,\mathrm{m}}}\, r_{y_{E,\mathrm{m}}}\, r_{H_{\mathrm{m}}}\, r_{x_{E,\mathrm{g}}}\, r_{y_{E,\mathrm{g}}}]^T \in \mathbb{R}^{10}$ is the measurement noise vector, with covariance matrix $R_k \in \mathbb{R}^{10\times 10}$.

4 Methodology

To obtain a smooth state estimate and to deal with changes in GPS noise, some adaptive state estimation algorithms are studied. The adaptive algorithms are used whenever a new GPS measurement is available, otherwise, the standard UKF is employed. Figure 1 illustrates the architecture of the state estimator based on the available sensors.

4.1 Unscented Kalman Filter

Recent works (Julier and Uhlmann, 2004; Arasaratnam and Haykin, 2009) demonstrated the improved accuracy of unscented Kalman filters over traditional extended Kalman filter (EKF) with competitive processing time. Instead of analytically or numerically linearizing (1)-(2) and using the Kalman filter equations, the *unscented Kalman filter* (UKF) employs the unscented transform (UT).

The UKF is a two-step state estimator, whose *forecast* step is given by

$$\{\hat{x}_{k|k-1},\, P^{xx}_{k|k-1},\, \hat{y}_{k|k-1},\, P^{yy}_{k|k-1},\, P^{xy}_{k|k-1}\} = \mathrm{Forecast}\Big(\hat{x}_{k-1|k-1},\, P^{xx}_{k-1|k-1},\, u_{k-1},\, f,\, h,\, Q_{k-1},\, R_k\Big) \quad (10)$$

and the *data-assimilation* step is given by

$$\{\hat{x}_{k|k},\, P^{xx}_{k|k},\, \nu_{k|k-1}\} = \mathrm{DataAssimilation}\Big(\hat{x}_{k|k-1},\, P^{xx}_{k|k-1},\, y_k,\, P^{yy}_{k|k-1},\, P^{xy}_{k|k-1}\Big) \quad (11)$$

where $\nu_{k|k-1} = y_k - \hat{y}_{k|k-1}$ is the innovation with covariance $P^{yy}_{k|k-1}$ and cross-covariance $P^{xy}_{k|k-1}$. For brevity, the detailed equations of UKF are not presented here, but they are found in (Julier and Uhlmann, 2004). The UKF parameters were set as in (Arasaratnam and Haykin, 2009).

4.2 Adaptive Filters

In many practical scenarios, the stochastic properties of the system vary depending on factors like environmental conditions and vehicle dynamics. In these cases, it is reasonable to think that the process and measurement noise matrices (Q_k and R_k) used in the Kalman filter might vary too.

Therefore, we investigate two adaptive approaches to consider time-varying noise statistics, namely (i) scaling approach and (ii) interact multiple model (IMM). Both adaptive methods use the information available in the *innovation*

$$\nu_k \triangleq y_k - \hat{y}_{k|k-1} \quad (12)$$

where $\hat{y}_{k|k-1}$ is the output estimate given by *data-assimilation* step of the UKF.

4.2.1 Gain Scaling

The algorithm presented in (Hide et al., 2004) is used to scale the noise covariance by the factor

$$s_k \triangleq \frac{\nu_k^T \nu_k}{\frac{1}{N}\sum_{j=k-N}^{k-1} \nu_j^T \nu_j}, \tag{13}$$

which is based on the relationship between the innovation (12) at the current time k and the N previous values.

In this work, when the innovation ν_k increases regarding the N previous values, we scale R_k as

$$R_k^s \triangleq \max\left(s_k,\, 1\right) R_k. \tag{14}$$

Then we replace R_k by R_k^s in the UKF equations and obtain the *adaptive unscented Kalman filter by covariance scaling* (AUKF-CS). As our purpose is to treat erroneous GPS measurements, we modify only the GPS components of R_k.

4.2.2 Interacting Multiple Model Filter

Figure 2 schematically illustrates the Interacting Multiple Model (IMM) estimator (Bar-Shalom et al., 2004). In this work, IMM considers a switching system described by a discrete set of 2 models, denoted by $M = \{M^1, M^2\}$. Model 1 considers reliable GPS measurements, whereas Model 2 considers unreliable GPS measurements. Both models differ by different values of R_k.

Assuming the knowledge of the prior probability γ_0^i for each model and the probabilities of switching from model i to j given by the transition matrix Π_{ij}, at each iteration, for $i, j = 1, 2$, the mixing probabilities $w_{k-1|k-1}^{i|j}$ are used for mixing the prior state estimates $\hat{x}_{k-1|k-1}^i$ and the prior covariance matrices $P_{k-1|k-1}^{xx,i}$. The mixed states $\hat{x}_{k-1|k-1}^{0,j}$ and covariance $P_{k-1|k-1}^{xx,0,j}$ are used as inputs for a bank of two UKFs, where each filter addresses a model. The output of each model-matched filter is the model-conditioned state estimate $\hat{x}_{k|k}^j$, the associated covariance $P_{k|k-1}^{xx,j}$, the model-conditioned innovation ν_k^j and its covariance $P_{k|k-1}^{yy,j}$. The model-conditioned innovation and its covariance are used to compute the likelihood function $\rho_j(\nu_k^j)$ of each model, which in turn, is used to update the model probabilities γ_k^j. Finally, the updated model probabilities are used to combine the model-conditioned estimates and covariances. The detailed equations of IMM are not presented here for shortness, but they are found in (Bar-Shalom et al., 2004, pp. 453-460).

4.3 Kalman Smoother

To improve the estimation and mitigate the effect of slowly sampled data, a smoother algorithm can

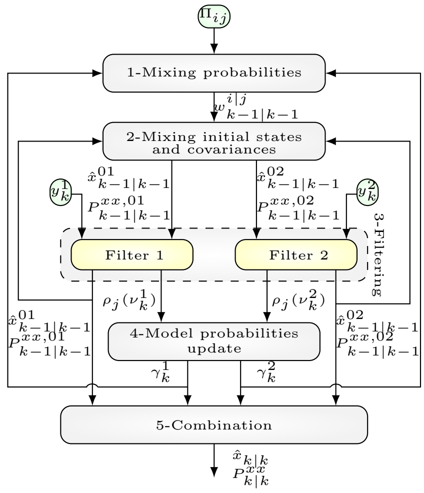

Figure 2: Block diagram of the IMM algorithm.

be used. The smoothers use the entire measurement data set over a fixed interval. Basically, they are used to estimate the states using the future measurements, y_{k+1}, y_{k+2}, ..., y_N, where N is the total length of data array, in addition to current and past data y_1, y_2, ..., y_k.

We use the two-filter approach, which is perhaps the most straightforward smoothing algorithm and was first suggested in (Fraser and Potter, 1969). The two-filter approach for smoothing obtains two estimates for the state vector x_k. The first estimate, $\hat{x}_{k|k}^f$, is based on the filtering algorithm given in Section 4.1, for instance. The second estimate, $\hat{x}_{k|k}^b$, is based on the same filter running backward in time from N to 0. The backward filter uses of the following model

$$\dot{x}(-t) = f\left(x(-t),\, u(-t), w(-t),\, -t\right), \tag{15}$$

$$y_{-k} = h\left(x_{-k},\, -k\right) + v_{-k}, \tag{16}$$

where $-t$ and $-k$ denote the time inversion of input and output data. For simplicity, we discretized (15) as we did before for the forward filter.

Next, the smoother combines the results of the forward and backward filters as follows

$$P_{k|k}^{xx,s} = \left((P_{k|k}^{xx,f})^{-1} + (P_{k|k}^{xx,b})^{-1}\right)^{-1}, \tag{17}$$

$$\hat{x}_{k|k}^s = P_{k|k}^{xx,s}\left((P_{k|k}^{xx,b})^{-1}\hat{x}_{k|k}^b + (P_{k|k}^{xx,f})^{-1}\hat{x}_{k|k}^f\right) \tag{18}$$

where $\hat{x}_{k|k}^s$ is the smoothed state mean with covariance $P_{k|k}^{xx,s}$. Note that, for this approach, any filter algorithm can be used for forward and backward steps.

5 Experimental Results

We now compare the performance of the aforementioned algorithms by using experimental flight data collected during a session of Red Bull Air

Race (RBAR). The RBAR World Championship is an international series of races with the participation of at least eight pilots at each race. The objective is to navigate in an aerial racetrack, delimited by air-filled pylons, called air gates, in the smallest possible time. The engines and propellers are standard for all teams. Thus, the pilots and their team dedicate their efforts to perfecting airframe aerodynamics, improve the pilot skills and plan the best path to follow during the race.

In this work localization and flight path reconstruction were performed. At this point, the importance of the adaptive approach and the inclusion of vision information must be clarified. During the air race, due to the aggressive maneuvers of the airplane and the environment noise caused mainly by the digital television transmitter installed on the aircraft, the GPS-information becomes unreliable. Thus, to improve the accuracy of estimate, the vision information is used. Also, in order to address the variation in the reliability of the GPS, the adaptive methods presented in Section 4 are tested.

From Section 4, we test the following algorithms: *Filter 1*, which only corresponds to the standard UKF, in this case, the GPS measurements are used; *Filter 2*, which corresponds to the AUKF-CS; and *Filter 3*, corresponding to the IMM approach. For path reconstruction, the smoother algorithm is employed. Three smoother algorithms (1, 2 and 3) are tested, each one using one of the aforementioned filtering algorithms. In our graphs and table, we differ among the approaches that use vision information from others by adding "$+ G$" to the original name.

For all tests the same configuration was adopted. We set $Q_{2,k-1} = \text{diag}(I_{2\times2}, 64\times10^{-4}, 16\times10^{-6}I_{4\times4}, 0.5I_{3\times3}, 4\times10^{-6}I_{3\times3}, 10^{-10}I_{3\times3})$ and $P_{0|0}^{xx} = 5Q_{2,k-1}$. The initial condition $\hat{x}_{0|0}$, the diagonals of $Q_{1,k-1}$ and R_k are defined from information provided by instrumentation. For the filter and smoother based on IMM algorithm, two models are used. The difference between models 1 and 2 is in the covariance matrix R_k. In model 2 the GPS components are multiplied by 100 to represent the case in which GPS is unreliable. Finally, for these same algorithms, we set $\gamma_0^i = [0.5\,0.5]^T$ and $\Pi_{ij} = \begin{bmatrix} 0.96 & 0.04 \\ 0.04 & 0.96 \end{bmatrix}$.

5.1 Localization and Path Reconstruction

Figure 3 shows the aircraft path estimated by the filtering and smoothing algorithms, respectively. It can be noted a deviation from the race path in some points, where the vehicle should be close to the gates, for instance when the airplane passes through gates 6 and 7. When the vision information is employed, abrupt corrections on the position occur. Note also that the smoothing algorithm yielded a smoother path estimate, mitigating the abrupt changing caused by GPS and vision information. Regarding the adaptive algorithms, *Filter 3* identifies that the GPS is unreliable between the gates 5 and 8, in the first lap, and between gates 5 and 1, in the second lap (see the zoomed-in detail of Figure 4). *Filter 1* and *Filter 2* yielded similar results, relying on GPS information. Due to similarity with the results already presented, some paths estimated by the filtering and smoothing algorithms (1, 2 and 3) are not shown in Figures 3.

Figure 5 illustrates two performance indexes. The first one measures the accuracy of estimation, computed by the error $\hat{e}$, which is defined as the Euclidean distance between the estimated position and the gate localization. The second index reflects the change in uncertainty by plotting the 0.99 confidence ellipses. It was verified that the gate localization is contained inside the confidence region only for Filter 3 and Smoother 3, when the vision information is employed. A reduction of uncertainty of estimation is noticeable when smoothing algorithms are used instead of the filtering algorithms. Furthermore, for all algorithms, a reduction of uncertainty and an improvement in the accuracy of estimation is noted when the vision information is employed, for instance, the average reduction of $\hat{e}$ was 86%, 87% and 96% for *Filter 1*, *2* and *3*, respectively. Table 1 shows the accuracy index for all algorithms for one lap of race. It is also noted that, the smoother algorithms were not effective, except for the *Smoother 3* which yielded an average improvement of 39% without vision information and 27% with vision information.

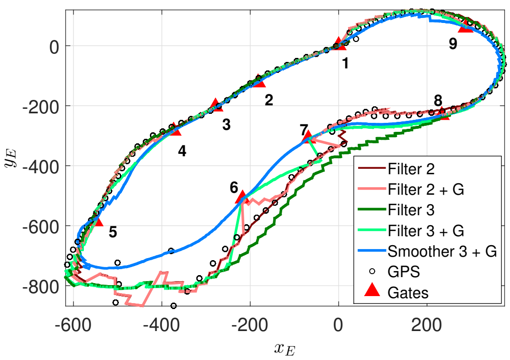

Figure 3: Aircraft paths estimated by the filtering and smoothing algorithms.

6 Concluding Remarks

In this paper, adaptive Kalman filters are presented as an alternative to treat the localization problem in GPS-unreliable environments. These algorithms can deal with changing of statistical properties of measurements models. We also propose the inclusion on vision information obtained from the vehicle on board camera to improve the

Table 1: Accuracy index $\hat{e}$ (m), computed by the distance between the estimated position and the gate localization. For each gate, the worst result is presented in italics and the best result in boldface.

Algorithm	Gate 1	Gate 2	Gate 3	Gate 4	Gate 5	Gate 6	Gate 7	Gate 8	Gate 9	Average
Filter 1	26,88	14,32	3,74	36,32	29,22	118,22	75,07	36,45	30,06	41.00
Smoother 1	37,35	19,27	2,89	42,85	*35,12*	106,11	61,53	40,25	26,46	41.30
Filter 2	26,87	14,40	3,76	36,42	29,21	116,93	75,08	36,42	*32,19*	41.26
Smoother 2	37,34	19,72	2,73	*43,02*	35,09	105,38	59,00	38,64	27,06	40.89
Filter 3	26,88	13,97	*3,76*	37,80	29,20	*215,40*	*117,01*	36,88	28,19	56.57
Smoother 3	*37,36*	*19,39*	3,11	37,53	30,78	80,24	29,23	*45,44*	26,29	34.38
Filter 1 + G	3,04	2,08	0,47	6,09	4,42	15,62	11,05	3,41	3,00	5.46
Smoother 1 + G	5,28	2,63	0,70	6,03	4,67	14,17	8,17	5,45	3,69	5.64
Filter 2 + G	3,03	2,05	0,47	5,29	4,42	15,46	11,08	3,40	2,57	5.31
Smoother 2 + G	5,27	2,62	1,39	5,63	4,68	14,08	8,19	4,89	3,51	5.58
Filter 3 + G	3,04	1,92	**0,46**	1,85	**4,18**	1,79	0,89	0,67	2,72	1.95
Smoother 3 + G	**1,59**	**1,06**	2,08	**1,11**	4,44	**0,59**	**0,35**	**0,35**	**1,22**	1.42

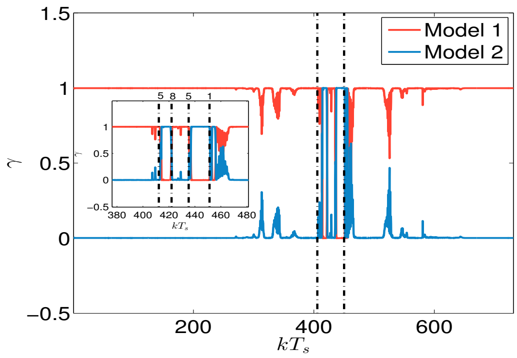

Figure 4: Model probability. In Model 1 the GPS measurements are considered reliable, and in Model 2, the GPS measurements are considered unreliable. The vertical black dashed lines delimit the race period.

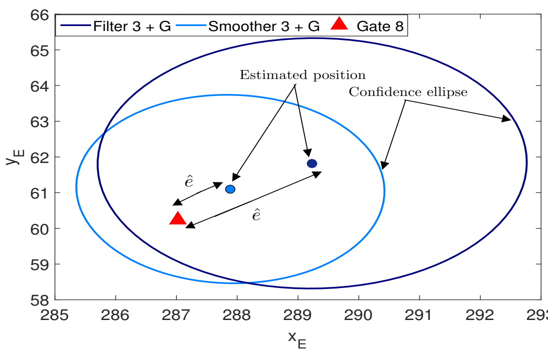

Figure 5: Illustration of two performance indexes. The uncertainty in estimated position is depicted by plotting the 0.99 confidence ellipse. The index $\hat{e}$ is computed by distance between the estimated position and the gate position.

localization when GPS information is unreliable or unavailable.

Experimental results indicate a performance improvement when the IMM approach is employed, which was able to detect unreliable GPS measurements. On the other hand, the gain scaling approach did not yield significant improvements with respect to position estimate when compared to the standard UKF. The vision information proved to be a good alternative when GPS measurements become unreliable.

Acknowledgments

The authors are grateful to Brazilian agencies CNPq, CAPES and FAPEMIG for financial support and Prof. Paulo Iscold for providing the experimental data.

References

Abuhashim, T. S., Abdel-Hafez, M. F. and Al-Jarrah, M. A. (2010). Building a robust integrity monitoring algorithm for a low cost GPS-aided-INS system, *International Journal of Control, Automation and Systems* **8**(5): 1108–1122.

Arasaratnam, I. and Haykin, S. (2009). Cubature Kalman filters, *IEEE Transactions on Automatic Control,* **54**(6): 1254–1269.

Bachrach, A., Winter, A. D., He, R., Hemann, G., Prentice, S. and Roy, N. (2010). RANGE - robust autonomous navigation in GPS-denied environments, *IEEE International Conference on Robotics and Automation (ICRA)*, pp. 1096–1097.

Bar-Shalom, Y., Li, X. R. and Kirubarajan, T. (2004). *Estimation with applications to tracking and navigation: theory algorithms and software*, John Wiley & Sons.

Beard, R. W. and McLain, T. W. (2012). *Small unmanned aircraft: Theory and practice*, Princeton University Press.

Chambers, A., Achar, S., Nuske, S., Rehder, J., Kitt, B., Chamberlain, L., Haines, J., Scherer, S. and Singh, S. (2011). Perception for a river mapping robot, *International Conference on Intelligent Robots and Systems (IROS)*, pp. 227–234.

Fraser, D. and Potter, J. (1969). The optimum linear smoother as a combination of two optimum linear filters, *IEEE Transactions on Automatic Control,* **14**(4): 387–390.

Hide, C., Moore, T. and Smith, M. (2004). Adaptive Kalman filtering algorithms for integrating GPS and low cost INS, *PLANS 2004. Position Location and Navigation Symposium,* pp. 227–233.

Hu, C., Chen, W., Chen, Y. and Liu, D. (2003). Adaptive Kalman filtering for vehicle navigation, *Journal of Global Positioning Systems,* **2**(01): 42–47.

Julier, S. J. and Uhlmann, J. K. (2004). Unscented filtering and nonlinear estimation, *Proceedings of the IEEE,* **92**(3): 401–422.

Jwo, D. J. and Tseng, C. H. (2011). Interacting multiple model nonlinear filter design for ultra-tightly coupled integrated navigation, *Control Conference (ASCC), 2011 8th Asian*, pp. 1294–1299.

Leutenegger, S. and Siegwart, R. (2012). A low-cost and fail-safe inertial navigation system for airplanes, *IEEE International Conference on Robotics and Automation (ICRA)*, pp. 612–618.

Shen, S., Mulgaonkar, Y., Michael, N. and Kumar, V. (2014). Multi-sensor fusion for robust autonomous flight in indoor and outdoor environments with a rotorcraft MAV, *IEEE International Conference on Robotics and Automation (ICRA)*, pp. 4974–4981.

Teixeira, B. O. S., Tôrres, L. A. B., Iscold, P. and Aguirre, L. a. (2011). Flight path reconstruction - A comparison of nonlinear Kalman filter and smoother algorithms, *Aerospace Science and Technology,* **15**(1): 60–71.

Terra, G. S., Tôrres, L. A. B. and Teixeira, B. O. S. (2014). Attitude estimation using a two-step unscented approach with gyro bias estimation and acceleration correction, *XX Congresso Brasileiro de Automática*, pp. 3421–3428.